The Three-Dimensional Chaotic Transport and the Great Ocean Barrier

HUIJUN YANG

Department of Marine Science, University of South Florida, St. Petersburg, Florida

ZHENGYU LIU

Department of Atmospheric and Oceanic Science, University of Wisconsin—Madison, Madison, Wisconsin

(Manuscript received 17 June 1996, in final form 23 December 1996)

ABSTRACT

The aim of this paper is to renew interest in the Lagrangian view of global and basin ocean circulations and its implications in physical and biogeochemical ocean processes. The paper examines the Lagrangian transport, mixing, and chaos in a simple, laminar, three-dimensional, steady, basin-scale oceanic flow consisting of the gyre and the thermohaline circulation mode. The Lagrangian structure of this flow could not be chaotic if the steady oceanic flow consists of only either one of the two modes nor if the flow is zonally symmetric, such as the Antarctic Circumpolar Current. However, when both the modes are present, the Lagrangian structure of the flow is chaotic, resulting in chaotic trajectories and providing the enhanced transport and mixing and microstructure of a tracer field. The Lagrangian trajectory and tracer experiments show the great complexity of the Lagrangian geometric structure of the flow field and demonstrate the complicated transport and mixing processes in the World Ocean. The finite-time Lyapunov exponent analysis has successfully characterized the Lagrangian nature. One of the most important findings is the distinct large-scale barrier—which the authors term *the great ocean barrier*—within the ocean interior with upper and lower branches, as remnants of the Kolmogorov–Arnold–Moser (KAM) invariant surfaces. The most fundamental reasons for such Lagrangian structure are the intrinsic nature of the long time mean, global and basin-scale oceanic flow: the three-dimensionality and incompressibility giving rise to chaos and to the great ocean barrier, respectively. Implications of these results are discussed, from the great ocean conveyor hypothesis to the predictability of the (quasi) Lagrangian drifters and floats in the climate observing system.

1. Introduction

The three-dimensional structure of Lagrangian flow pathways in the world oceans lies at the very heart of our understanding of the ocean climate and World Ocean's role in the earth's climate variability. The understanding of long-term transfer of freshwater, salt, heat, and tracers or materials of biogeochemical importance such as nutrients and carbon by the global and basin-scale oceanic flow all crucially depends upon the knowledge of the three-dimensional structure of the Lagrangian flow pathways in the oceans. What are the characteristics of the Lagrangian trajectories or flow pathways in a three-dimensional, long time averaged global and basin-scale oceanic flow? The great ocean conveyor hypothesis (Broecher 1991) provides a very useful conceptual model for the global ocean Lagrangian flow pathways. For example, the upper Atlantic Ocean is characterized by a northward transport of warm, salty water to the subtropical and subpolar North Atlantic where air–sea processes result in the formation of various components of North Atlantic Deep Water (NADW). The colder NADW is then advected southward, at depth, to complete the meridional overturning circulation. [See Schmitz and McCartney (1993) for an excellent review in the Atlantic Ocean circulation.] However, this is an over simplified picture of the Lagrangian flow pathways that may not even hold in the long time mean. There are two major modes of the basin-scale circulation in all world major oceans. One is the wind-driven gyre circulation mode and the other is the thermohaline circulation mode driven by the buoyancy force. These two modes are believed to contribute equally to the net northward water mass transport in the upper Atlantic, even though they are interrelated to each other and their interplay is very complicated. However, even for such a simple flow, its Lagrangian information remains unexplored. For example, what is the geometric structure of Lagrangian pathways in a simple, long time mean, three-dimensional, basin-scale flow consisting of both gyre and meridional overturning circulation mode?

Recent studies showed the great complexity of the Lagrangian trajectories, transport, and mixing in a two-

Corresponding author address: Dr. Huijun Yang, Department of Marine Science, University of South Florida, 140 Seventh Ave. S., St. Petersburg, FL 33701-5016.
E-mail: yang@marine.usf.edu

dimensional, time-dependent gyre-scale oceanic flow. The resulting chaotic transport and mixing can explain the water mass intergyre exchange, the potential vorticity homogenization, and the associated water property front aligned with the Gulf Stream (Yang and Liu 1994; Liu and Yang 1994; Yang 1996a,b,c). The results demonstrated that the chaotic transport and mixing by gyre-scale circulation could be the dominant mechanism for water mass transport and tracer mixing in the gyre-scale ocean. These results are of great interest to oceanographers, in general, because the Lagrangian chaos by such a simple, laminar large-scale flow can give considerably enhanced transport and mixing, and microstructure for tracer, without any turbulence or eddies in the flow field and any tracer diffusivity in the usual sense. Moreover, the large-scale flow is relatively simpler to be dynamically understood and accurately measured than, for example, eddies and small-scale motions.

The Antarctic Circumpolar Current (ACC) plays an important role in the global ocean circulation and ocean climate. One of the major distinctions between the three-dimensional, steady ocean circulation in a basin, say the North Atlantic or North Pacific Ocean, and the steady ACC is that the long term averaged ACC can be assumed to be zonally symmetric. On the other hand, because of the lateral boundary, the long term averaged flow in an ocean basin is intrinsically three-dimensional [e.g., for the North Atlantic, see Schmitz and McCartney (1993)]. What is the major difference in terms of the Lagrangian structure between these two long term averaged, idealized three-dimensional, steady flow fields?

The chaotic Lagrangian structure by a simple, laminar flow, such as two-dimensional, time-dependent gyre-scale circulation (Yang and Liu 1994; Yang 1996a,b), means that infinitesimally close fluid particles following the Lagrangian trajectories or streamlines may separate exponentially in time, while remaining in a bounded domain, and that individual trajectories may appear to fill entire regions of space. Thus, the positions of fluid particles may become effectively unpredictable after a finite period of time.

The use of (quasi) Lagrangian floats or drifters in the oceanographic field research program (see U.S. WOCE 1995 for the latest) and possibly in the ocean circulation prediction operation, as one of important components of the earth's climate observing system, has been greatly increased recently in part because of the popularity of satellite tracking systems. However, only very limited floats or drifters are deployed and tracked for a limited time. For the best utilization of the limited float and drifter data a better understanding of the Lagrangian structure of the oceanic flow becomes more urgent. Two related questions have to be addressed: How accurately can the floats or drifters data from the observation and modeling studies represent the Lagrangian structure of the flow in general? For example, how accurately can we interpret these limited data for the ocean model comparison and validation and translate them into the Eulerian flow information as the ocean model initial data input? To simplify the problem, we can ask an equivalent but inverse question. For a given, simple, laminar, large-scale Eulerian oceanic flow field, such as a steady, three-dimensional, basin-scale flow, how accurately can we predict its Lagrangian trajectories and the Lagrangian structure?

The purposes of the present paper are 1) to examine the Lagrangian structure of a simple steady basin-scale oceanic flow, 2) to highlight the potential importance of its implications for the three-dimensional Lagrangian flow pathways, water mass transformation, enhanced transport, and mixing in the World Ocean and for the drifters and floats data, and 3) to renew interest in the Lagrangian view of ocean circulations and its implications in physical and biogeochemical ocean processes. In this paper, we explore the complexity of the Lagrangian structure in such a simple, three-dimensional flow. We show that the Lagrangian flow pathways and the transport are chaotic and that there is a large-scale barrier to the chaotic transport in the basin, called the *great ocean barrier*. The three-dimensionality and incompressibility of the steady global and basin-scale flow are the fundamental reasons for such Lagrangian structure, giving rise to the chaos and the great ocean barrier, respectively.

The paper is arranged as follows. The simple ocean model is formulated in section 2. The Lagrangian structure along with several examples of Lagrangian trajectories is given in section 3. Section 4 shows how a passive tracer field can be redistributed by this simple oceanic flow field. Section 5 presents the Lyapunov exponent distribution, which characterizes the Lagrangian structure. Section 6 is devoted to discussions.

2. Ocean model

a. The double gyre–thermohaline circulation

The basin-scale model ocean is assumed to have a square basin with a flat bottom:

$$0 \le x \le 2L, \; -L \le y \le L, \; -H \le z \le 0,$$

where L and H are the horizontal scale and depth of the ocean basin; x, y, and z denote the eastward, northward, and upward variables, respectively. The long time mean horizontal circulation is assumed to be a steady double-gyre wind-driven circulation with a subpolar gyre to the north and a subtropical gyre to the south. The streamfunction can be written as

$$\psi_W = (x - 2)\,\mathrm{curl}\tau(y)(1 - e^{-x/\delta_S}), \qquad (2.1)$$

where the wind curl is $\mathrm{curl}\tau = \sin(\pi y)$ and the variables are nondimensionalized by the horizontal scale L. Hence, the gyre circulation consists of the interior Sverdrup flow and the western boundary current, with the Stommel boundary layer width δ_S. The long time mean

meridional overturning circulation is a steady single buoyancy-driven thermohaline cell with a narrow sinking branch against the northern wall and a wide upwelling branch in the rest of the basin. The nondimensionalized streamfunction is

$$\psi_B = \psi_{BI}(y, z)[1 - e^{(y-1)/\delta_B}], \tag{2.2}$$

with the interior thermohaline flow, given by $\psi_{BI}(y, z) = (y + 1)B(z)$ and the buoyancy forcing distribution $B = \epsilon \sin(\pi z/b)$, where the $\epsilon(>0)$ represents the strength of the buoyancy-driven flow relative to that of the wind-driven flow and $b = H/L$ is the aspect ratio; δ_B is the width of the sinking branch. The total three-dimensional, long time averaged oceanic flow field in the dimensionless form is given by

$$(u, v, w) = \left(-\frac{\partial \psi_W}{\partial y}, \frac{\partial \psi_W}{\partial x} + \frac{\partial \psi_B}{\partial z}, -\frac{\partial \psi_B}{\partial y}\right), \tag{2.3}$$

where u, v, and w are the zonal, meridional, and vertical component of the three-dimensional oceanic flow velocity, respectively. From consideration of meridional transport in the interior the strength of the thermohaline circulation should have the same order magnitude as that of the gyre circulation mode and b and ϵ should have the same order of magnitude. For example, if we choose $L = 2000$ km and $H = 4$ km, then ϵ has to be order of b ($= 0.002$). Therefore, the vertical motion due to the overturning mode is 500 times weaker than that of the gyre mode. Equivalently we can choose $b = \epsilon = 1$ for simplicity of computation and presentation without loss generality. Figure 1 shows the flow field, where and hereafter the following parameter values have been chosen, $\delta_S = 0.025$, $\delta_B = 0.01$, $b = 1$, and $\epsilon = 1$. These values are consistent with present estimates.

Obviously this is a highly idealized ocean model and is far from the reality of the World Ocean. Nevertheless, this kinematic model mimics several important aspects of real oceans. First, this flow satisfies the continuity equation $u_x + v_y + w_z = 0$ and thus conserves the water mass automatically. Second, the wind-driven gyre circulation mode and the meridional overturning mode are both representative of the real ocean with the western boundary current and northern boundary sinking (as shown in Fig. 1). These major features are consistent with our current understanding of basin-scale transport (e.g., Schmitz and McCartney 1993). Third, this flow can produce a realistic sea surface temperature (SST) pattern through redistribution process (not shown, but see the tracer field below). However, as emphasized in the introduction, the purpose here is to highlight the possible consequence of a simple, steady, three-dimensional, basin-scale flow from the Lagrangian point of view, and is not to validate the ocean model. Such a kinematic approach has been succesufully applied in many oceanographic studies [see Yang (1996b) for a more complete reference].

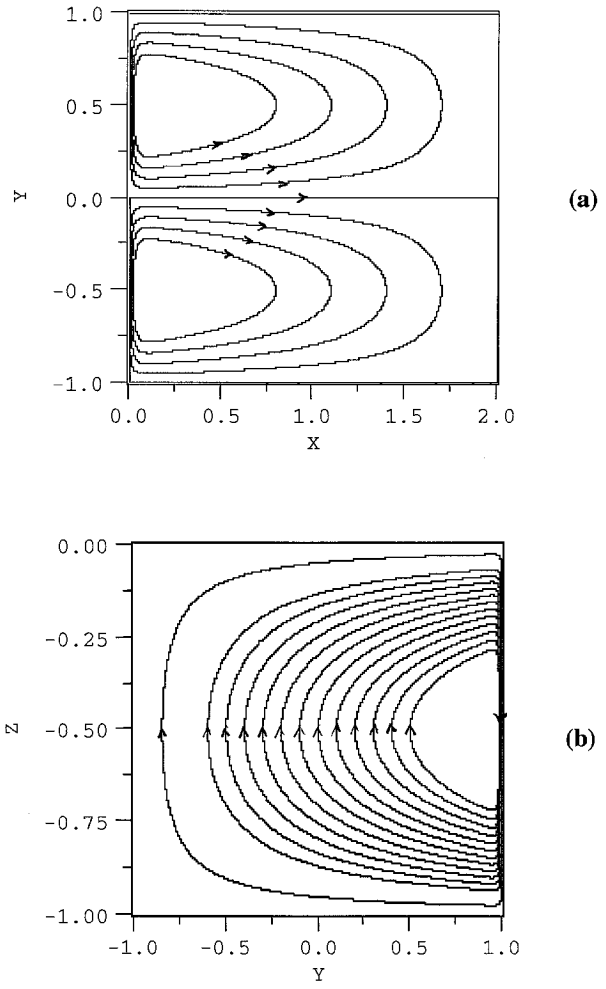

FIG. 1. The three-dimensional, steady, basin-scale flow fields. (a) The wind-driven gyre mode on the horizontal plane and (b) the meridional overturning circulation mode on the meridional–vertical plane.

b. Equations for the Lagrangian trajectory

The Lagrangian trajectories, or flow pathways of fluid parcels, with different initial positions can be found by solving the following three ordinary differential equations in the ocean basin:

$$\frac{dx}{dt} = u(x, y, z), \qquad \frac{dy}{dt} = v(x, y, z),$$

$$\frac{dz}{dt} = w(x, y, z). \tag{2.4}$$

This constitutes a three-dimensional, autonomous dynamical system. A very important advantage of this model is that the oceanic flow is laminar and in analytic form so that there could be no error associated with the turbulence and numerical difference scheme. Such errors cannot be avoided and are often hard to estimate when the flow field is obtained by numerically solving

the governing nonlinear equations. Here, the only possible numerical error is solely due to the integration of the ordinary differential equations. Moreover, this error can be completely controlled to the desired level, for example, by simply reducing the time step of integration in a finite period of time.

3. The Lagrangian trajectories

When the flow consists of only one of the two modes, the flow is two-dimensional and steady. Such a flow cannot generate chaotic Lagrangian trajectories because it constitutes a two-dimensional dynamical system. A dynamical system consisting of two autonomous ordinary differential equations cannot behave chaotically (Guckenheimer and Holmes 1983). However, if the oceanic flow consists of both the gyre and the meridional overturning mode, the Lagrangian trajectories and flow pathways can either be chaotic or nonchaotic, depending on the origin of the fluid parcels, that is, the initial conditions.

Figure 2 show some examples of the three-dimensional Lagrangian trajectories and flow pathways generated by this three-dimensional, steady flow. The total integration time is 4 in nondimensional time unit; one time unit is about a decade in dimensional timescale in the present system. It is seen that the Lagrangian trajectories could be regular, or nonchaotic, when originating in some place within the intermediate layer (Fig. 2a), that is, the so-called great ocean barrier (to be explained shortly). The four fluid parcels start in the western intermediate layer on $z = -0.5$, along $y = -0.2$ in the interval of $x = 0.2$ to $x = 0.4$. They rise northward and eastward to the northern basin boundary near the surface and then almost vertically sink to near the bottom of the ocean. Then they move back to the south along the near-bottom and rise again back to the north, to the northern basin boundary layer below the ocean surface. There they vertically sink to near the bottom and move southward along the bottom eastern boundary to near the southern basin boundary. They then rise eastward to the western boundary below the surface and continue their course to the north. They meridionally circulate three times and circulate in the subtropical gyre one time in the whole course (see Fig. 2a for details). The four Lagrangian trajectories always stay together, and, in fact, they stay closer together after the first time that they rise from near bottom. Hence these Lagrangian trajectories are not chaotic.

Figure 2b showed four Lagrangian trajectories originating in the upper-central subtropical gyre. The four fluid parcels first stay together, moving toward the north and sinking to near the bottom at the northern basin boundary and then flowing toward the south along the near-bottom, reaching the southern basin. After reaching the western boundary layer near the ocean bottom, they continue moving together toward the west and north. The fluid parcels then rise upward and eastward and start to separate from each other while spiraling upward. They depart from each other greatly after the second meridional loop as shown in red. They are not as regular as the previous example, and, therefore, may be called almost nonchaotic.

The chaotic examples of the Lagrangian trajectories of the fluid parcels come from the fluid parcels originating in the upper Labrador Sea and the Florida Current (Figs. 2c,d). The fluid parcels originating in the upper Labrador Sea first circulate in the western region and sink down to near the bottom (Fig. 2c). They then move along the bottom western boundary current to the south and spiral upward around the subtropical western recirculation center three times before moving upward and northward to the north, to the northern basin boundary, sinking down to near the bottom. When they move back to the south, one of them returns to the north and the rest move all way to the south and then rise upward and westward, taking similar pathways as the previous one (Fig. 2b). Examples of the fluid parcels in the Florida Current are most dramatic (Fig. 2d). After reaching the northern basin boundary, sinking down to the ocean bottom and moving back the south, the trajectories spiral five times around the subtropical western recirculation center upward and then move to the north. At the end of integration, three parcels are found in the subtropical gyre and one in the subpolar gyre. They are not regular at all. In fact, they are totally chaotic in the sense of dynamical systems theory (to be discussed in section 5).

4. Tracer mixing experiments

To better understand the physics of the transport and mixing processes in such three-dimensional, steady, basin-scale circulation, we conducted direct Lagrangian experiments to model the passive tracer mixing. The evolution of the tracer mixing is due to the three-dimensional advection of the flow field; that is,

$$\frac{dC}{dt} = Q + \kappa\nabla^2 C, \tag{4.1}$$

where $C = C(x, y, z, t)$ is the tracer concentration (or perturbation) field along the Lagrangian trajectories, determined by Eq. (2.4), and Q and κ are tracer source function and diffusivity, respectively. One of advantages of this Lagrangian approach is that there is no artificial diffusivity in the Lagrangian modeling. In fact, the tracer diffusivity can be zero. A large artificial tracer diffusivity is always present in the conventional numerical modeling (see Yang 1996c for detailed discussion). For simplicity, we assume the tracer to be nondiffusive and conservative with $Q = \kappa = 0$ in this study.

In order to examine the meridional mixing, we further assume that the initial tracer is independent of the depth and is a linear function of y, for example, $C_0(y) = C(x, y, z, t = 0) = y$. The high concentration or value (red color) in the subtropical gyre and lower concentration or value (purple color) in the subpolar gyre. The three-

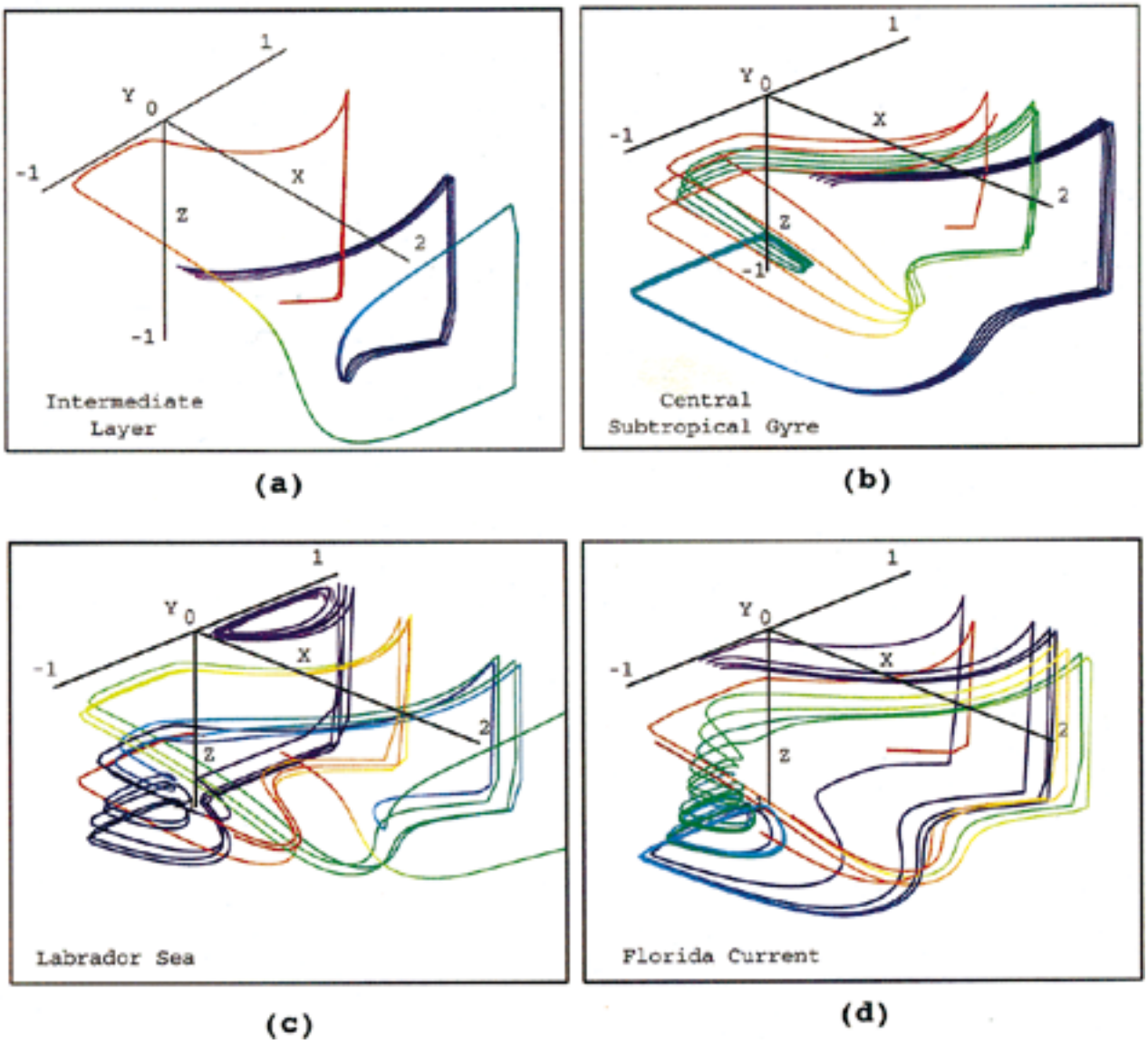

FIG. 2. Some examples of the three-dimensional Lagrangian trajectories of the double-gyre-thermohaline oceanic flow. The trajectories are (a) nonchaotic when originating in the intermediate layer near (0.3, −0.2, and −0.5) in the great ocean barrier; (b) almost nonchaotic when originating in the upper central subtropical gyre near (1, −0.5, −0.2); (c) chaotic when originating in the upper Labrador Sea near (0.01, 0.8, −0.05); and (d) chaotic when originating in the Florida Current near (0.01, −0.5, −0.01). The color of the trajectory represents the time, from purple to red as the time increases.

dimensional tracer distributions were shown in Figs. 3a,b, whereas the isosurfaces of tracer field were shown in Figs. 3c,d after $t = 0.5$. Due to the three-dimensional flow advection, the tracer field undergoes dramatic change and the mixing process is very complicated. For example, the water of subtropical origin (red-yellow) has been spread throughout the basin with thin sheet structure (Fig. 3c), whereas the water near intergyre boundary origin has also been spread throughout both gyres and from top to bottom (Fig. 3d).

In order to examine the vertical mixing process, we conducted the same experiment with a different initial condition (Fig. 4). In this experiment, the initial tracer concentration or value is assumed to be independent of y and is linear function of the depth, for example, $C_0(z) = C(x, y, z, t = 0) = -z$. The upper-layer tracer has

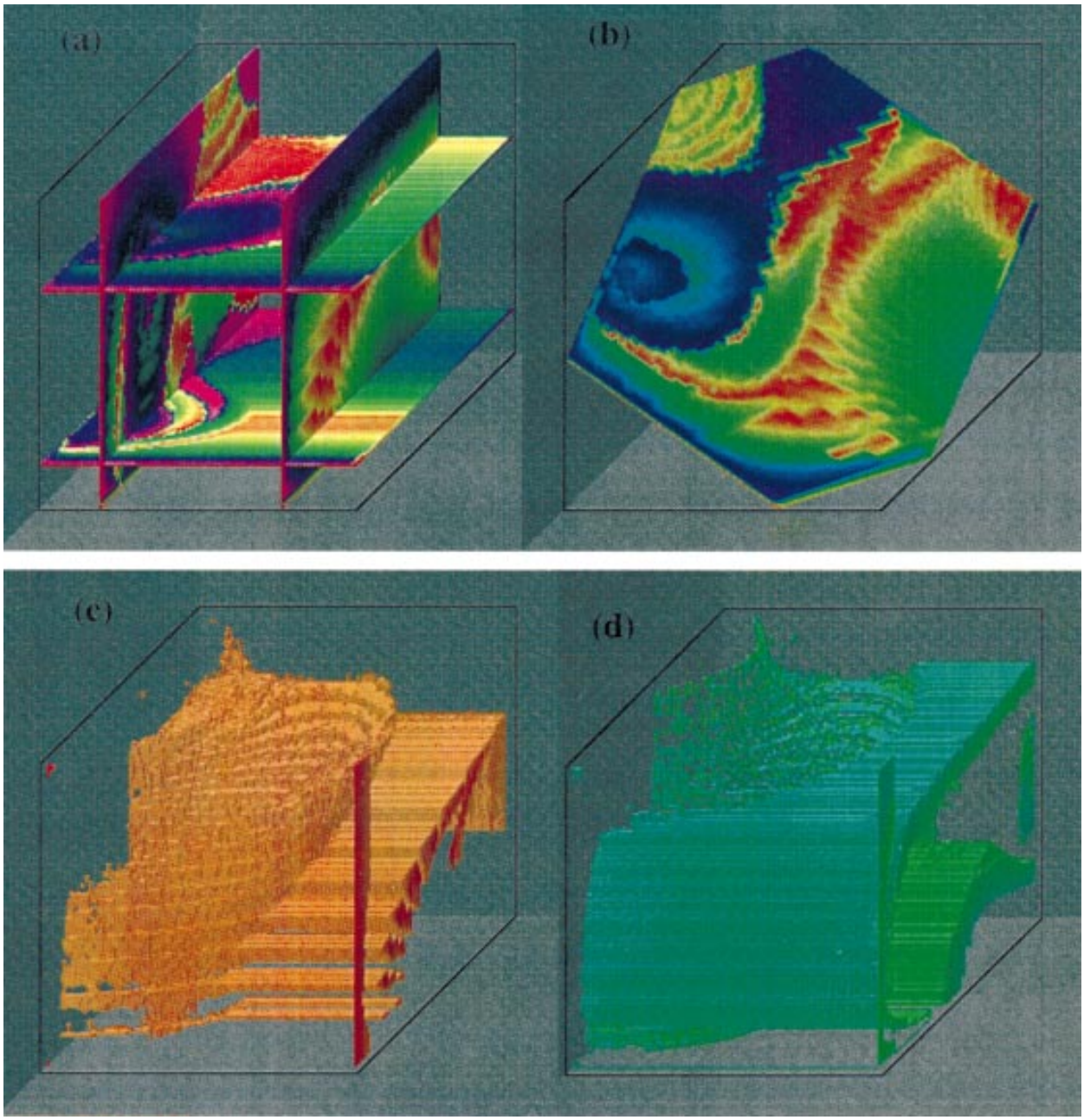

FIG. 3. The tracer distributions at $t = 0.5$. The initial tracer is linearly distributed in y with high value (red color) in the subtropical gyre and low value (purple color) in the subpolar gyre: (a) and (b) Tracer distributions, and (c) and (d) the three-dimensional isosurface of the tracer with different values.

high concentration or value (red color) and the lower-layer tracer has lower concentration or value (purple color). The results after $T = 0.5$ were shown in Figs. 4a,b for tracer distributions and in Figs. 4c,d for isosurfaces.

As the tracer mixing processes continue, it was clearly observed that there are some almost no-mixing regions mingled within well-mixing regions (Fig. 5 for $t = 2$). There are microstructures in the tracer field due to the chaotic mixing processes as well as the large-scale barriers to mixing. The stretching and folding processes are most strikingly evident. The stretching and folding provides an enhanced mixing for the tracer field.

5. The great ocean barrier: The Lyapunov analysis

A better way to distinguish the chaotic behavior from the regular, or nonchaotic, behavior of these Lagrangian

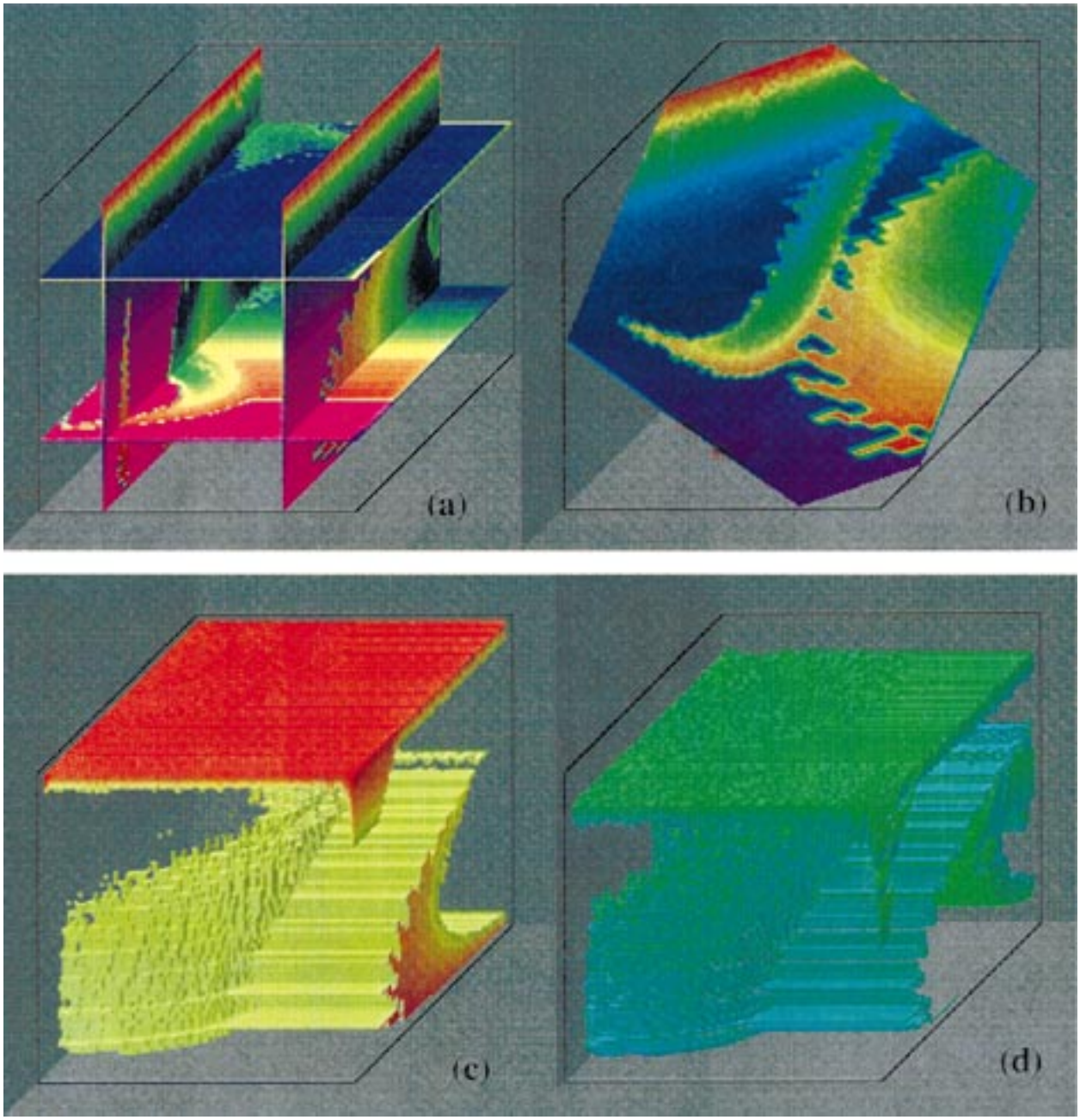

FIG. 4. The tracer distributions at $t = 0.5$. The initial tracer is linearly distributed in z with high value (red color) in the upper layer and the low value (purple color) in the lower layer: (a) and (b) tracer distributions, (c) and (d) the three-dimensional isosurface of the tracer with different values.

trajectories and the tracer mixing process in the dynamical systems theory is through calculating the Lyapunov exponent. The Lyapunov exponent provides a qualitative and quantitative characterization of dynamical behavior; it is a measure of the exponentially fast divergence or convergence of nearby trajectories in the phase space of the underlying dynamical system (Guckenheimer and Holmes 1983; Ott 1993). The trajectories are the Lagrangian fluid parcel trajectories and the phase space in this dynamical system is exactly the three-dimensional geometric space of the ocean basin. A system with one or more positive Lyapunov exponents is defined to be chaotic. Given a continuous dynamical system in an n-dimensional phase space, we monitor the evolution of an infinitesimal n-sphere of initial conditions; the sphere will become an n-ellipsoid due to the

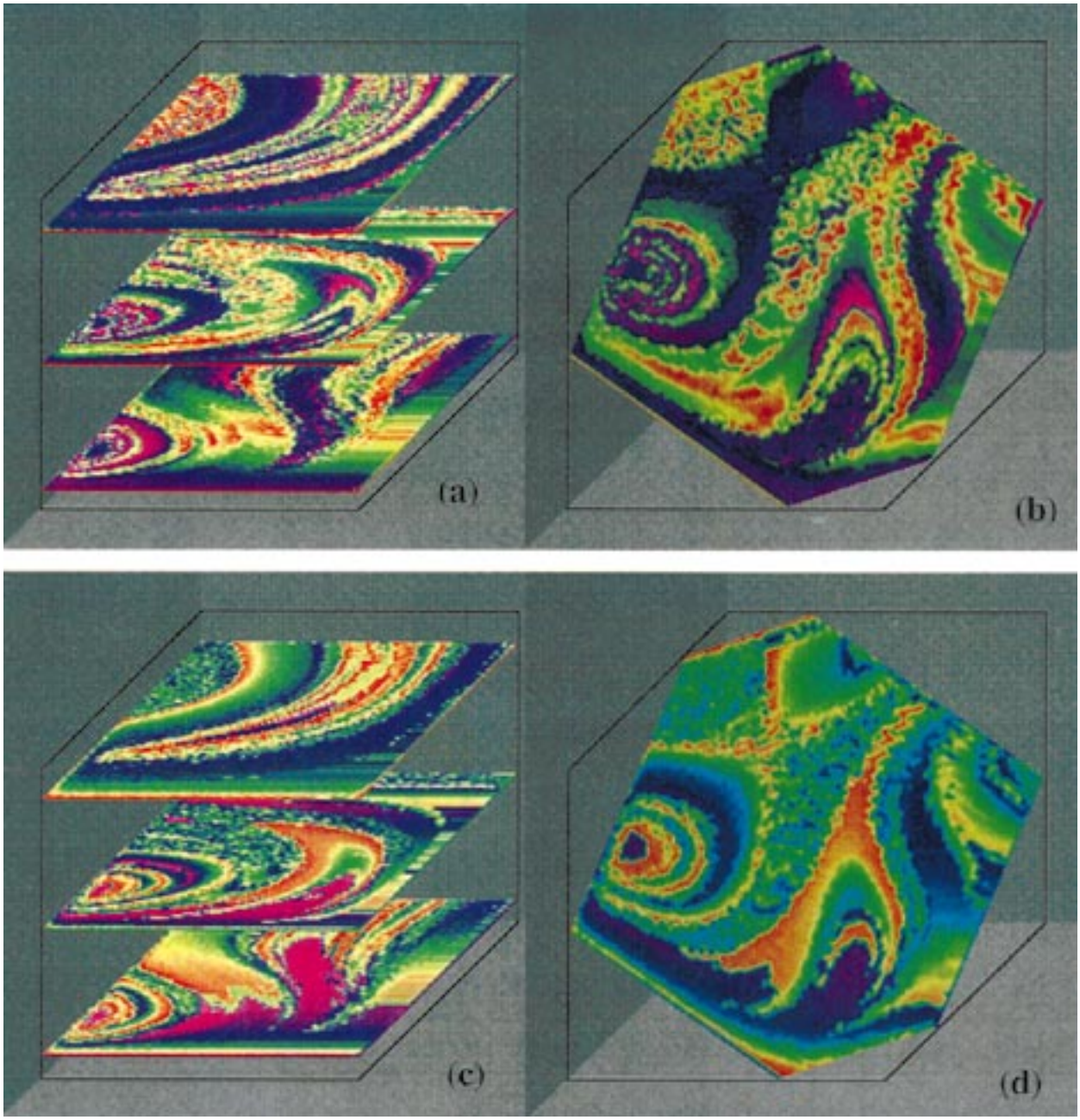

FIG. 5. The tracer distributions at $t = 2$ for (a) and (b) the case as in Fig. 3 and (c) and (d) the case as in Fig. 4.

locally deforming nature of the flow. The largest one-dimensional Lyapunov exponent is then defined in terms of the length of the ellipsoid principal axis $p(t)$:

$$\lambda = \frac{1}{\lim t\to\infty} \frac{1}{t} \log_2 \frac{p(t)}{p(0)}. \tag{5.1}$$

There is a standard computational method of the Lyapunov exponent calculation for the system consisting of ordinary differential equations (e.g., Guckenheimer and Holmes 1983; Wolf et al. 1985; Ott 1993). However, we are more interested in the behavior of the Lagrangian trajectory in a finite period of time. We could modify the method by taking a finite period of time instead of infinity to compute the finite-time Lyapunov exponent for the present system. Another method has also been successfully used to calculate the finite-time Lyapunov exponent for a two-dimensional, unsteady gyre-scale oceanic flow (Yang 1996a,b).

Figure 6 shows the finite-time Lyapunov exponent distributions on a horizontal plane near the ocean surface (the top panel), the intermediate layer (the middle panel), and near the bottom (the bottom panel) after two nondimensional unit time.[1] It was seen that one of the most striking features is the high positive Lyapunov exponent value in the Labrador Sea and the western boundary current, including the Florida Current. Hence, the Lagrangian trajectories originating from these regions are chaotic. The conclusion is in complete agreement with the previous Lagrangian trajectories in Fig. 2c,d. The region in the central domain has no positive Lyapunov exponent including the central subtropical gyre. Hence, the Lagrangian trajectories originating from this region are regular or nonchaotic. This agrees well with Fig. 2b. The southern boundary region is also chaotic. In the intermediate layer on $z = -0.5$, the subpolar gyre is very chaotic as well as western boundary layer (see the lower left panel of Fig. 6). The most striking feature is the much lower value zonal region in the south side of the intergyre boundary. The nearby Lagrangian trajectories would stay together all times. This represents a nonchaotic barrier to the chaotic transport and mixing. A typical example is shown in Fig. 2a. Again the Lyapunov exponent has successfully identified this barrier. The Lyapunov exponent distributions near the ocean bottom are given in the lower right panel in Fig. 6, showing a chaotic region in the eastern boundary and some chaotic layer among the nonchaotic layer.

The distributions on the vertical–zonal cross section are given in Fig. 7, whereas those on the vertical–meridional cross section are shown in Fig. 8. It was found that in the middle subpolar gyre meridional cross section, the western region and most of the middle ocean are chaotic, whereas there are two zonal nonchaotic zones in the upper layer and the other in the lower layer, respectively. The lower layer is more chaotic than the upper layer except at the western boundary in the subtropical gyre.

The most striking feature that emerges from the Lyapunov exponent calculations is the distinct large-scale ocean barrier to the chaotic transport and mixing, called the *great ocean barrier*. The barrier rises near the bottom in the northern basin boundary toward the south, continues upward and southward to the center of the basin, then goes back northward and upward and finally approaches the northern basin boundary just below the surface in the midbasin.

The similarity between the Lagrangian tracer mixing experiments in Figs. 3–5 and that in the Lyapunov exponent in Figs. 6–8 is most evident. However, the tracer mixing experiment can only qualitatively show the mixing process, whereas the Lyapunov exponent can quantitatively characterize the mixing process. Hence, the Lyapunov exponent analysis supports evidence from previous Lagrangian trajectories and tracer mixing experiments, arguing that there is a great ocean barrier to mixing.

The Lyapunov analysis does not provide only quantitative information about the fluid parcel pathways or trajectories: this analysis also comes into its own in discussions on the microstructure of the tracer field. For example, consider the fate of a small sphere of fluid tracer of size L_0 placed at a point in the ocean with Lyapunov exponent λ. After time T, the tracer parcel has stretched out to a cylindrical filament of length $L_0 \exp(\lambda T)$ in the one direction and radius $L_0 \exp(-\lambda T/2)$ or a disk sheet of radius $L_0 \exp(\lambda T)$ with thickness $L_0 \exp(-2\lambda T)$. Taking a typical value $\lambda = 2$ per unit time, $T = 2$, and $L = 100$ km, a filament 5459 km long of radius 13.5 km, or a disk sheet of radius 5459 km with thickness 0.335 cm, is obtained; after $T = 4$, these numbers become 298 096 km and 1.8 km for the filament or 298 096 km and 1.1×10^{-4} cm for the sheet! Because of the length of the filament or the huge sheet, it becomes highly contorted, as in Figs. 2–5. In particular, the isosurfaces in these figures illustrate vividly the thin contorted sheet structure (Figs. 3 and 4). Therefore, the simple, laminar, three-dimensional basin-scale steady flow is very capable of producing the microstructure of the tracer field in the world oceans.

If the concentration gradient of the tracer is initially ∇C_0 at the starting point of the fluid parcel, then the gradient after time T is $\nabla C_0 \exp(\lambda T)$ (Varosi et al. 1991). If the initial gradient field of the tracer is rather smooth and uniform in space, then after some time has passed, the tracer gradient field consists of an interwoven set of filamentary and sheet structures. The long filaments or large thin disk sheets (corresponding to points with high value of the Lyapunov exponent) support the highest gradients and are most contorted, while weak gradients are supported on relatively short filaments or small sheets. Therefore, this steady, laminar, three-dimensional flow can indeed greatly enhance the tracer transport and mixing in the global or basin-scale oceans. Moreover, it has been shown that the spatial variability of Lyapunov exponent is also directly related to the fractal and multifractal formalism. As a means of describing spatially complex system, this formalism has attracted a great deal of attention recently (e.g., Varosi et al. 1991; Ott 1993 and references therein). Hence, the Lyapunov analysis does provide a better means for describing this complicated structure.

6. Discussion

The Lagrangian flow pathways or trajectories of the three-dimensional, steady global- and basin-scale oce-

[1] The largest exponent should always be zero or positive theoretically in the present system since it is a conservative or nondissipative dynamic system. The negative values shown here are solely due to the finite-time calculation, and they approach zero as the time increases. Therefore, the region with negative value should be interpreted as regular or nonchaotic region.

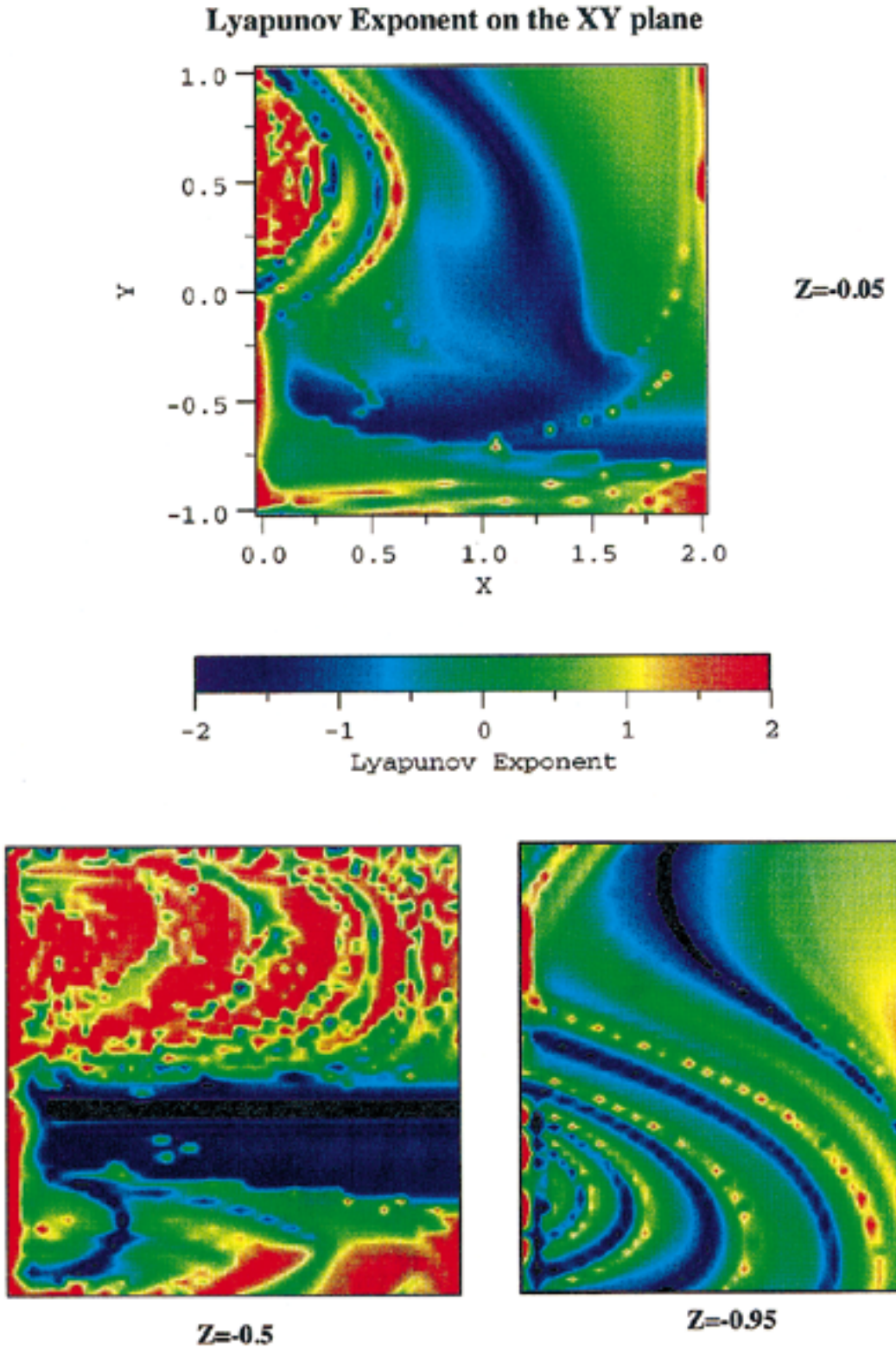

FIG. 6. The finite-time Lyapunov exponent distributions for a horizontal level plane (a) on the near surface at $Z = -0.05$, (b) on the intermediate level at $Z = -0.5$, and (c) on the near bottom at $Z = -0.95$. The high positive value indicates the strong chaotic region, whereas the low or zero value represents the nonchaotic region or barrier to chaotic transport.

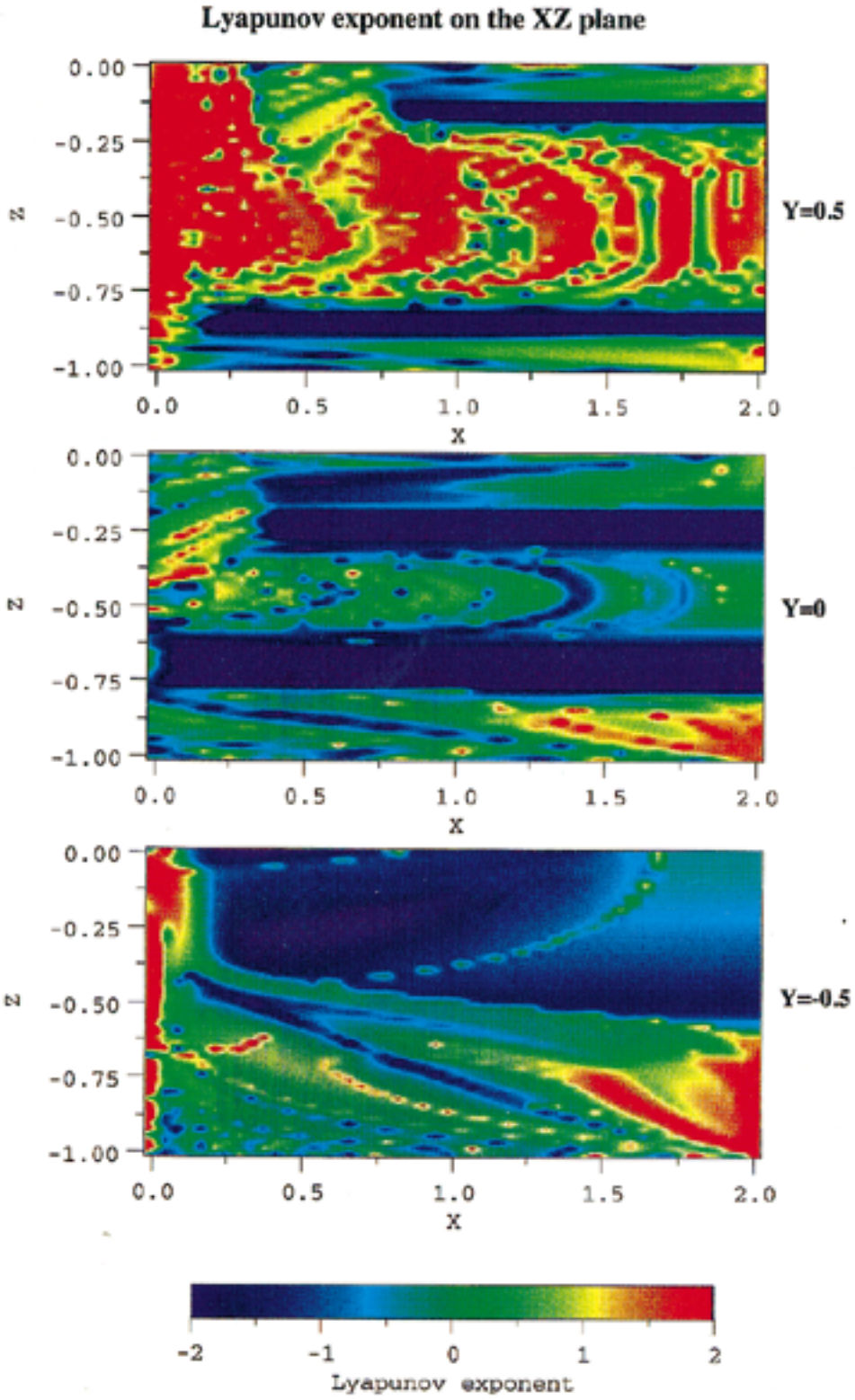

FIG. 7. The finite-time Lyapunov exponent distributions in the zonal–vertical plane (a) along the midsubpolar gyre at $y = 0.5$, (b) along intergyre boundary at $y = 0$, and (c) along the midsubtropical gyre at $y = -0.5$.

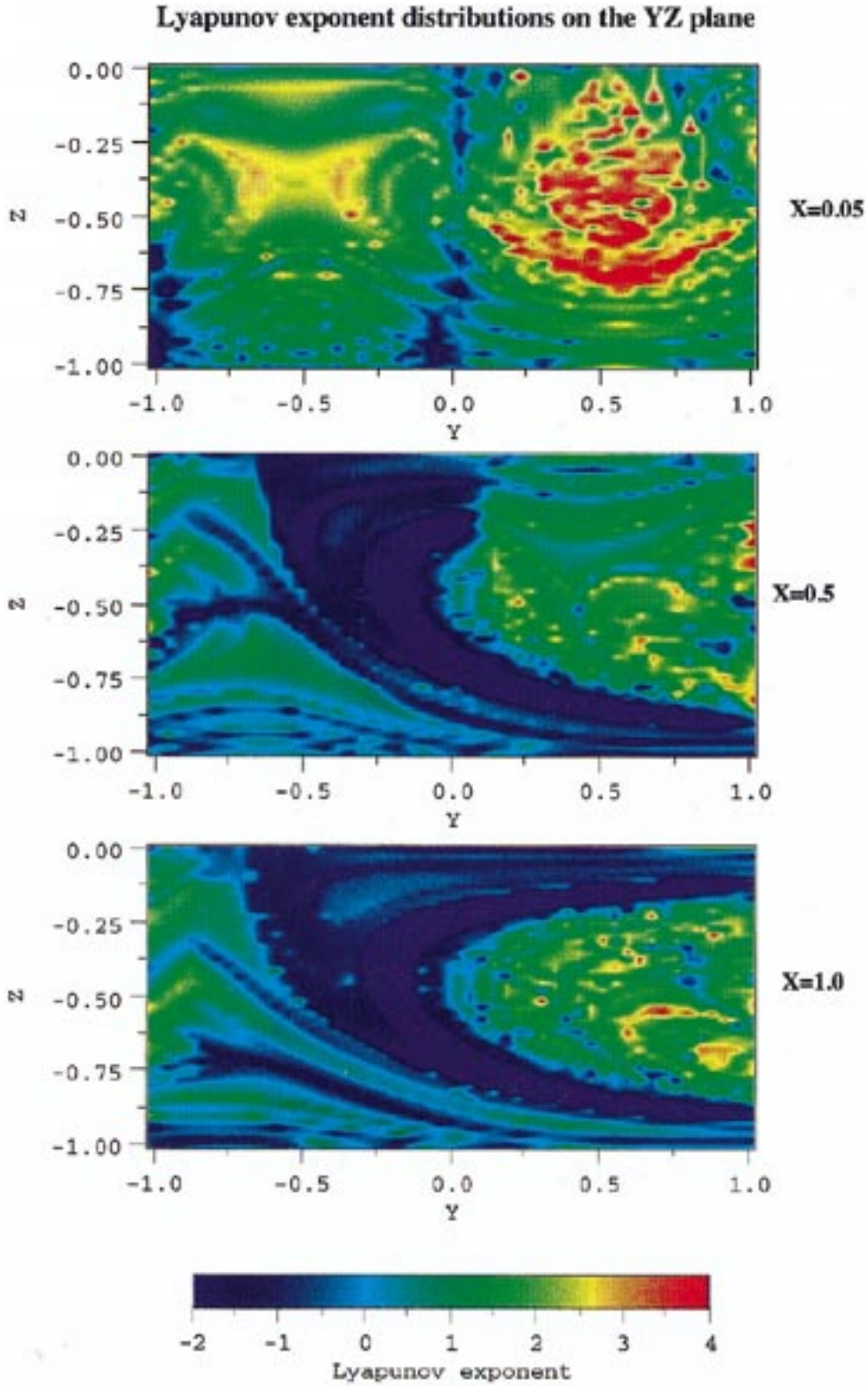

FIG. 8. The finite-time Lyapunov exponent distributions on the meridional–vertical plane (a) near the western boundary at $x = 0.1$, (b) along the midwestern basin at $x = 0.5$, and (c) along the center of the basin at $x = 1$.

anic flow could be either nonchaotic or chaotic, sensitively depending upon the initial locations of the fluid parcels. This kind of simple flow can provide the enhanced transport and mixing and microstructure for tracer without turbulence or eddies in the flow field, in the usual sense, limited only by a large-scale ocean transport barrier. The Lagrangian structure of its trajectories and the tracer mixing process can be better characterized by the Lyapunov exponent spatial distributions. All these analyses identify the large-scale barrier to the transport and mixing in the interior of the basin, called the great ocean barrier.

a. Three-dimensionality and incompressibility

Such behavior of the Lagrangian trajectories by basin-scale oceanic flow is due to its intrinsic nature: three-dimensionality and incompressibility. The Lagrangian trajectories cannot be chaotic if a steady basin-scale flow is two-dimensional. It is, therefore, the three-dimensionality of steady global and basin oceanic flow that gives rise to chaos in its Lagrangian structure. Because of the incompressibility of the fluid flow, the total divergence of this oceanic flow is exactly zero. Unlike the Lorenz system (Lorenz 1963), it is not a dissipative system. Thus, the system cannot have any strange attractor as such the trajectories will not be attracted to a finite domain with zero volume. Instead, the ocean domain can have both chaotic and nonchaotic regions. Thus, it is the incompressibility of the flow that gives rise to the great ocean barrier.

Even though the particular model used in this study is far from reality, the three-dimensionality and incompressibility are two generic features for all realistic global and basin-scale oceanic flows. Therefore, the present model is a generic one and conclusions reached here are expected to hold in general to some extent (but also see § 6g).

b. The great ocean conveyor

Because of the fundamental nature of the global and basin-scale oceanic flow, the Lagrangian structure of the flow is chaotic. Thus, the water masses may chaotically transfer from one place to another, especially in the western boundary current and intergyre boundary current. The regular, steady Lagrangian flow pathways, hypothesized in the great ocean conveyor (Broecher 1991), thus, may be conceptually useful, but physically unlikely, even over a very long timescale. In reality, the global oceanic flow is three-dimensional and time dependent. The time-dependence in the three-dimensional flow may greatly modify the Lagrangian structure, making it more complicated than that observed here (see section 6g for more discussion). Therefore, the probability that a fluid particle may travel throughout the great ocean conveyor may not be significantly greater than through any other path.

c. The ACC

In contrast, the long time mean, three-dimensional ACC is similar to the basin-scale flow except without eastern and western boundary effects. The kinematic ACC can similarly assume the following form for the wind-driven part:

$$\psi_W = \text{curl}\tau(y), \tag{6.1}$$

and the buoyancy-driven thermohaline cell assumes the same form:

$$\psi_B = \psi_{BI}\,[1 - e^{(y-1)/\delta_B}]. \tag{6.2}$$

The total three-dimensional, steady ACC flow is given by

$$(u, v, w) = \left(-\frac{\partial\psi_W}{\partial y}, \frac{\partial\psi_B}{\partial z}, -\frac{\partial\psi_B}{\partial y}\right). \tag{6.3}$$

A counterpart in the atmosphere for such a flow is the zonally symmetric Hadley cell. The Lagrangian trajectories are the solutions of

$$\frac{dx}{dt} = u(y), \qquad \frac{dy}{dt} = v(y, z), \qquad \frac{dz}{dt} = w(y, z), \tag{6.4}$$

with periodic zonal domain.

Even though the ACC has three components in the velocity field, this flow is fundamentally different from the double gyre–thermohaline circulation model [Eq. (2.3) or Eq. (2.4)]. There is a zonal symmetry in the flow field so that the distance of a Lagrangian trajectory from its original position is independent of its zonal axis. The first of the three equations is decoupled from the other two equations. This system, thereby, is essentially a two-dimensional, continuous dynamical system and their Lagrangian trajectories cannot be chaotic. Therefore, we expect to observe relatively regular drifter trajectories in the ACC system. The ACC acts as a barrier for chaotic transport and mixing in the global ocean circulation.

Thus, the probability that a fluid particle may travel throughout the ACC is significantly greater than throughout the great ocean conveyor. Unlike in the ACC, the presence of eastern and western boundaries breaks the zonal symmetry of the basin-scale ocean circulation, making the flow truly three-dimensional. Thus, the horizontal boundaries of the ocean basins are of great importance to Lagrangian pathways. The results also showed the extreme delicacy of the interplay between the gyre circulation mode and the meridional overturning mode in the global and basin-scale ocean. If either one of these modes is absent, the Lagrangian trajectory cannot be chaotic.

d. The KAM invariant surfaces and topology

For two-dimensional, time-periodic flows the Kolmogorov–Arnold–Moser (KAM) theorem (see, e.g., Arnold 1989) plays an important role. Namely, it provides sufficient conditions for the existence of invariant circules for the associated two-dimensional Poincare map

of the two-dimensional, time-periodic flow. These invariant circules act as barriers to transport and mixing. Some advance has been made recently concerning ''KAM-like'' theories for three-dimensional volume-preserving maps, for example, by Cheng and Sun (1990). The most celebrated three-dimensional, steady flow is the Arnold–Baltrami–Childress (ABC) flow (e.g., Dombre et al. 1986). This three-parameter family of spatially periodic flow is a simple steady-state solution of Euler's equations or of the Navier–Stokes equation with an appropriate force. The Lagrangian trajectories also have a complicated structure. In general, there is a set of closed helical streamlines or trajectories, each of which is surrounded by a finite region of KAM invariant surfaces (see, e.g., Guckenheimer and Holmes 1983; Ott 1993). The present three-dimensional, steady flow field is a kinematic model and not a solution of the nonlinear dynamical equation. It is possible to derive the three-dimensional flow field used here from linear dynamics of ocean physics. Nevertheless, the two systems do share the same features such as the nondivergence, integrable in the absence of some parameter and a perturbed Hamiltonian system. Hence, they both have chaotic and nonchaotic regions with a complicated Lagrangian structure.

The great ocean barriers found here also can be viewed as the analog of the KAM invariant surfaces. Even though the present system [Eq. (2.4)] itself is not a Hamiltonian system, it does share some properties with the perturbed Hamiltonian system. For example, the total divergence is zero. When $\epsilon = 0$ or ∞, the system is indeed an integrable Hamiltonian system with one degree of freedom. Thus, the system can be viewed as a perturbed Hamiltonian system.

To better understand the geometric structure of the Lagrangian trajectories in the current system, we consider the two simplified cases. First, if there is no meridional overturning mode, the flow is vertically uniform and the streamlines are horizontally wrapping up around an infinite number of vertical elliptic cylinders, whose center is located at one of two gyre centers. The elliptic cylindrical surfaces are the KAM invariant surfaces. If instead there is no gyre mode, the flow is zonally uniform and the streamlines are wrapping up in the meridional–vertical plane around an infinite number of zonally oriented elliptic cylinders, whose center is located at the center of the meridional overturning cell. The KAM invariant surfaces are the zonally oriented elliptic cylindrical surfaces. All Lagrangian trajectories are regular in either case, in the sense that they have to stay on their own KAM surface in space and cannot move from one KAM surface to another. Moreover, the Lagrangian trajectories cannot intersect themselves because the flow is steady. Hence, there is no chaos in either case. The present system with both the gyre and the meridional overturning mode can be viewed either as a perturbed first case, that is, the gyre system perturbed by the meridional overturning mode, or the perturbed second case, that is, the overturning system perturbed by the gyre mode. The perturbation makes the phase space of the Lagrangian trajectories truly three-dimensional, and, hence, leads to destruction of the KAM invariant surfaces and, thus, to chaos. The Lagrangian trajectories can move freely or chaotically. Therefore, it is three-dimensionality in the steady flow that makes the Lagrangian trajectories and their Lagrangian structure chaotic. However, the perturbation cannot in general destroy all original KAM invariant surfaces. What remains is what we call the great ocean barrier.

In contrast, in the ACC, the KAM invariant surfaces are the zonally oriented elliptic cylindrical surfaces, that is, the KAM tori, the Lagrangian trajectories can only move on their own KAM surface. There is, however, a difference between the KAM surfaces in the ACC and those in the above two cases. A careful examination reveals that in the above two cases the Lagrangian trajectories not only stay on their own KAM surface, but also stay at the same level (i.e., fixed z) for the first one and the meridion (i.e., fixed x) for the second one. In fact, the Lagrangian trajectories in the unperturbed system are closed lines on the respective planes. However, in the ACC, the Lagrangian trajectories can move along the KAM surface in the zonal direction with the velocity $u(y)$ depending on latitude. Nevertheless, no matter how much these trajectories may be able to wander, they have to stay on their own KAM tori and cannot intersect each other. Therefore, the Lagrangian trajectories and their Lagrangian structure in the zonally symmetric, steady ACC cannot be chaotic.

The stagnation points are critical in determining the location of chaotic region and the KAM surfaces. In the three-dimensional, basin-scale flow, in addition to the eight stagnation points on each corner of the basin, there may be an additional four pairs (eight) of stagnation points: one pair located in the subpolar side on the surface western boundary ($x = 0$, $z = 0$), the second pair located in the subtropical gyre on the bottom western boundary ($x = 0$, $z = -b$), the third pair located in the subtropical gyre on the surface eastern boundary ($x = 2$, $z = 0$), and the fourth pair located in the subpolar gyre on the bottom eastern boundary ($x = 2$, $z = -b$). The exact position of each of these stagnation points depends on the relative magnitude of the buoyancy and wind-driven flow. The Lagrangian trajectories originating near a hyperbolic point are likely to be chaotic, whereas an elliptic point is surrounded by the KAM surfaces.

e. Possible evidence for the great ocean barrier

Some evidence of the possible existence of the great ocean barrier may be indicated from tracer distributions in the North Atlantic Ocean. The ocean barrier to transport and mixing should correspond to a large tracer gradient due to lack of chaotic transport and mixing.

Observations show that there is some large tracer gradient within the upper and lower branches in the North Atlantic Ocean on the south–north section (Fig. 5 of Reid 1993). These tracers include salinity, oxygen, nitrate, phosphate, and silica. Obviously more studies are needed before we can verify the great ocean barrier hypothesis. On the other hand, as discussed above the model has some generic properties of the global and basin-scale ocean that are not dependent on the particularity of this model. Therefore, we are hopeful that we may be able to verify this hypothsis in the future by using a more realistic ocean model.

f. Predictability of Lagrangian drifter

This study raises a fundamental question about how accurately we can interpret the (quasi) Lagrangian floats or drifters data for the real oceanic flow, even though the present ocean model is far from the reality of world oceans. There are always limits on how many and how often drifters can be deployed, and how long one can monitor them. If we assume that these drifters truly represent fluid parcels, their trajectories are representative of the Lagrangian flow pathways. How accurately may the limited number of drifters and limited monitoring time represent the Lagrangian flow pathways, in general, over the region of interest? On what timescale may we use the Lagrangian information without problem? Our results suggest that in a three-dimensional, steady basin-scale flow field, if the drifters are deployed in the nonchaotic region, for example, in the ocean great barrier, the results will be sufficient for describing the flow field. On the other hand, if a limited number of drifters is deployed in the strong chaotic region, such as in the western boundary current, the interpretation of drifter data is rather complicated due to the chaotic nature of the trajectories, especially their fate. Therefore, more studies on how accurately Lagrangian drifter data really represents the flow field in a region and, for a given flow field, what are the characteristics and structure of its Lagrangian trajectories and tracer fields should be a high priority in physical oceanography.

The predictability of Lagrangian drifter or float can be measured by the Lyapunov exponent. The timescale of predictability τ can be defined by

$$\tau = \frac{1}{\lambda},$$

where λ is the Lyapunov exponent defined in (5.1). Suppose the flow advection timescale is 10 years. Since the average value of the Lyapunov exponent is only 1 to 2, the predictability timescale will be from 5 to 10 years, which may be longer than drifter monitoring time. Therefore, for global- and basin-scale flow, this problem may be less serious in observation. However, it may not be the case for strong current systems such as the western boundary current systems, the Gulf Stream, and the Kuroshio. There the currents may be ten or a hundred times stronger than the mean current in this model. As a result, the Lypunov exponent will be increased to ten or one hundred times. Accordingly, the predictability timescale of Lagrangian drifter or float in such strong current system becomes months or even a few days. This may become a serious problem. How best to sample drifters or floats and to interpret the drifter and float data in such systems should be carefully considered in the light of possible short predictability timescale of the drifters or floats.

g. Concluding remarks

A word of caution is in order. The real global and basin-scale ocean circulation has a large spectra of spatial and temporal variability. Three-dimensionality is certainly an important ingredient of the Lagrangian chaos, but time dependence (in particular, nonperiodic time evolution) certainly may play a crucial role as it does in two-dimensional ocean flow (e.g., Yang 1996a,b,c). Almost nothing is known about the time-dependent three-dimensional global or basin-scale oceanic flows, nor about the effect of dynamically active coherent structures on the properties of Lagrangian structure. For example, what happens to the KAM tori and hence the great ocean barrier? Will the time dependence and the dynamically active coherent structures destroy the KAM invariant surfaces? The dynamical system describing Lagrangian structure of time-dependent three-dimensional oceanic flow is similar to a Hamiltonian system with more than two degrees of freedom. For a Hamiltonian system, there is a striking difference between the chaos encountered in systems with two degrees of freedom and that encountered in systems with more than two degrees of freedom. Using topological arguments, Arnold (1964) showed that, for systems with two degrees of freedom, the chaotic layers are interconnected to form a web that is dense in the phase space. For initial conditions on the web, chaotic motion is driven along the layers, leading to a global diffusion not constrained by the KAM invariant surfaces. This mechanism is commonly called Arnold diffusion. Our system is not a Hamiltonian system but shares some properties of a Hamiltonian system. Will there be Arnold diffusion like in the Lagrangian structure of the time-dependent three-dimensional oceanic flow? What are their implications for the great ocean barrier and the enhanced transport and mixing? Definitely further studies are needed to answer these questions and to assess how much the conclusions reached here have to be modified when either the time dependence or the dynamically active coherent structure is taken into account in the three-dimensional large-scale oceanic flow.

Finally, the present work employed the simplest possible ocean model in which both the major ocean circulation modes are included. The model is a good first-order basin-scale model, in particular for the North Atlantic. We may derive this model from linear dynamics

of basin-scale ocean physics. But how robust will this kinematical model based on a three-dimensional steady-state prescription of the basin-scale basic flow be upon any small perturbation? This question remains to be answered. Obviously, this simplest possible ocean model is far from reality. It is also very desirable to use more realistic global- and basin-scale models in future study of the three-dimensional Lagrangian pathways and structure.

Acknowledgments. We are grateful to Drs. J. Pedlosky, W. Young, K. Bryan, J. Mahlman, and R. X. Huang for their encouragement and discussions. This work is supported in part by the ONR and the NSF.

REFERENCES

Arnold, V. I., 1964: Instability of dynamical system with several degrees of freedom. *Sov. Math. Dokl.,* **5,** 581–585.

——, 1989: *Mathematical Methods of Classical Mechanics.* 2d. ed. Springer-Verlag, 508 pp.

Broecker, W., 1991. The great ocean conveyor. *Oceanography,* **4,** 79–89.

Cheng, C. Q., and Y. S. Sun, 1990: Existence of invariant tori in three-dimensional measure-preserving mappings. *Celestial Mech.,* **47,** 275–292.

Dombre, T., U. Frisch, J. M. Greene, M. Henon, A. Mehr, and A. M Soward, 1986: Chaotic streamlines in the ABC flows. *J. Fluid Mech.,* **167,** 353–391.

Guckenheimer, J., and P. Holmes, 1983: *Nonlinear Oscillations, Dynamical Systems, and Bifurcations of Vector Fields.* Springer-Verlag, 451 pp.

Liu, Z., and H. Yang, 1994: The intergyre chaotic transport. *J. Phys. Oceanogr.,* **24,** 1768–1782.

Lorenz, E. N., 1963: Deterministic nonperiodic flow. *J. Atmos. Sci.,* **20,** 130–141.

Ott, E., 1993: *Chaos in Dynamical Systems.* Cambridge University Press, 385 pp.

Reid, J. L., 1993: On the total geostrophic circulation of the North Atlantic Ocean: Flow patterns, tracers, and transports. *Progress in Oceanography,* Vol. 33, Pergamon, 1–92.

Schmitz, W. J., and M. S. McCartney, 1993: On the North Atlantic circulation. *Rev. Geophys.,* **31,** 29–49.

U.S. WOCE, 1995: U.S. contribution to WOCE and ACCP: A program design for an Atlantic circulation and climate experiment, 112 pp. [Available from U.S. WOCE Office, College Station, Texas

Varosi, F., T. M. Antonsen, and E. Ott, 1991: The spectrum of fractal dimensions of passively convected scalar gradients in chaotic fluid flows. *Phys. Fluids,* **3A,** 1017–1028.

Wolf, A., J. B. Swift, H. L. Swinney, and J. A. Vastano, 1985: Determining Lyapunov exponents from a time series. *Physica,* **16D,** 285–317.

Yang, H., 1996a: The subtropical/subpolar gyre exchange in the presence of annually migrating wind and a meandering jet: Water mass exchange. *J. Phys. Oceanogr.,* **26,** 115–130.

——, 1996b: Chaotic transport and mixing by ocean gyre circulation. *Stochastic Modeling in Physical Oceanography,* R. Adler, P. Müller, and B. Rozovskii, Eds., Birkäuser, 439–466.

——, 1996c: The Lagrangian modeling of potential vorticity homogenization and the associated front in the Gulf Stream. *J. Phys. Oceanogr.,* **26,** 2480–2496.

——, and Z. Liu, 1994: Chaotic transport in a double gyre ocean. *Geophys. Res. Lett.,* **21,** 545–548.